# Marine Current Turbine Generator System with Induction Machine Growing Neural Gas (GNG) MPPT based on Sensorless Sea Speed Estimation

L. Greco, C. Testa
INSEAN-CNR
Rome, Italy
luca.greco@cnr.it , claudio.testa@cnr.it

M. Pucci, G. Vitale
ISSIA-CNR
Palermo, Italy
pucci@pa.issia.cnr.it ,
vitale@pa.issia.cnr.it

M. Cirrincione
The University of the South Pacific
Laucala Campus,Suva, Fiji Islands
m.cirrincione@ieee.org

*Abstract*— **This paper presents a MPPT technique for high performance marine current generator with induction machine based on the Growing Neural Gas (GNG) network. The marine turbine characteristic curve has been firstly predicted by a BEM hydrodynamic formulation. The BEM analysis has been compared with experimental results obtained at the QinetiQ cavitation tunnel (Haslar Marine Technology Park). For the experimental application, a back-to-back power converter configuration with two voltage source converters has been considered, one on the machine side and the other on the grid side. Each converter has been controlled with a high performance vector control technique, respectively Field Oriented Control (FOC) and Voltage Oriented Control (VOC). A test setup has been built for the experimental assessment of the methodology. Experimental results show the correct behaviour of the proposed MPPT technique which permits to instantaneously estimate the sea speed and correspondingly to compute the optimal machine reference speed for tracking the maximum available power.**

## I. INTRODUCTION

Marine Current Turbines (MCT) are playing a key role as renewable energy sources when the ocean or marine currents kinetic energy can be exploited. As a matter of fact, MCT can provide a regular and predictable energy resource [1]. Although, in principle, some concepts are common with the horizontal axis turbines used in wind energy systems, there are significant differences such as the effects of free surface and the occurrence of cavitation [2] that makes the integrated study of both hydrodynamics and electromechanical conversion issues very challenging.

In the last ten years several papers have been published, and many of them deal with the turbine design by numerical methods and with the experimental verification of the mechanical performance [1-9]. Recent studies have been focused on the generation of electric energy by rotating machines [10-12] and with the integration of such a source on an autonomous hybrid energy system [13]; however only few works address the issue of the Maximum Power Point Tracking (MPPT) without any flow sensor [14] and, among them, only simulation results have been presented.

This paper proposes a MPPT technique for a high-performance MCT generator with induction machine based on the growing neural gas (GNG) network. The GNG network has been trained off-line to learn the turbine torque versus water speed and machine speed characteristic surface. In the production phase the GNG retrieves the optimal generator reference speed (i.e., the speed that corresponds to the maximum extractable power) for any instantaneous value of the water speed. In this way the MPPT is achieved without any recursive algorithm, like all those belonging to the category of Perturbe & Observe (P&O) or Hill & Climb (H&C).

A similar approach has been successfully assessed for wind generators [15-17], both for fixed and variable pitch turbine blades, thus covering both the variable power and the constant (rated power) working regions. In this paper this approach is applied for learning the characteristics of a suitably designed turbine. Such a turbine has been investigated through a fully three-dimensional, steady hydrodynamic formulation based on a Boundary Element Method (BEM) suitable for the analysis of hydroloads acting upon lifting bodies in arbitrary motion in a potential flow. The BEM analysis has been compared with experimental results obtained at the QinetiQ cavitation tunnel (Haslar Marine Technology Park). As far as the electromechanical conversion chain and the generation towards the power grid are concerned, the behavior of the marine turbine has been emulated by a torque controlled Permanent Magnet Synchronous Motor (PMSM) drive, embedded in laboratory set-up. The adopted generation system is based on two

This paper has been funded by the following research projects: 1. RITmare, Ricerca ITaliana per il mare (Italian Research for the sea) CUP:B91J11000740001; 2. TESEO, Tecnologie ad alta Efficienza per la Sostenibilità Energetica ed ambientale On-board (High efficiency technologies for on-board energy and environmental sustainability) CUP: B61C12000850005; 3. CNR per il Mezzogiorno (Advanced Technologies for Energy Efficiency and Sustainable Mobility) CUP: B51J10001290001.

voltage source inverters (VSIs), in a back-to-back configuration scheme. A high-performance control of both the two VSIs has been adopted, particularly the FOC (Field Oriented Control) for the induction generator drive and the VOC (Voltage Oriented Control) for the grid-side inverter. The neural network has been used as a virtual measurement system of the sea speed, exploiting the peculiarity of the GNG to invert functions; it outputs the estimated sea speed from the actual machine torque and speed. On this basis and given the optimal tip speed ratio of the turbine, the computation of the optimal power reference speed is straightforward.

Finally, the whole conversion chain, including the induction generator, the back-to-back configuration with two voltage source converters one on the machine side and the other on the grid side, has been implemented in laboratory to assess the validity of the proposed technique.

## II. Marine Current Turbine Performance

The performance of the marine turbine have been herein evaluated by a fully three-dimensional (3D) free-wake panel method yielding the hydrodynamic loads upon blade(s) surface under the assumption of inviscid, incompressible and irrotational onset flow. Predictions from the proposed approach have proven to be accurate in terms of delivered power as long as the assumption of attached-flow holds [18 – 22], that is, for sectional angle of attacks up to 10-12 degrees. Within this range, viscosity-induced tangential stresses may be roughly modeled by the Blasius theory [23] and *Grigson* formula [24] for laminar and turbulent flows, respectively, by assuming that the boundary-layer developed on the blade surface behaves like that over a flat plate at Reynolds numbers matching turbine working-point. Throughout the paper, turbine performance analysis is performed in steady-state conditions since a constant rotor angular velocity and an incoming water flow, normal to the rotor-disk and uniformly distributed in space, are assumed. Steady-periodic conditions due to the presence of yaw angles or nonuniform distributions of the inflow, as well as unsteadiness related to the transient-state from variations of the angular velocity are intentionally not considered. This, however, does not affect the goodness of the results as far as the turbine analysis and consequent MPPT algorithm design is concerned. In the following the main aspects of turbine hydrodynamics are outlined; details may be found in [22].

### A. Panel Method Hydrodynamics: Background

Under the assumption of incompressible, inviscid and irrotational flow, the perturbation velocity potential field is governed by the Laplace equation that may be solved through the following Boundary Integral Representation everywhere in the field [25]:

$$E(\mathbf{x})\varphi(\mathbf{x}) = \oint_{S_B}\left(\frac{\partial\varphi}{\partial n}G-\varphi\frac{\partial G}{\partial n}\right)dS(\mathbf{y})-\int_{S_W}\Delta\varphi\frac{\partial G}{\partial n}dS(\mathbf{y}) \quad (1)$$

where $\mathbf{x}$ denotes a field point, $S_B$ the turbine surface, $S_W$ the convected wake, $\mathbf{n}$ the local unit normal and $\mathbf{y}$ a point located on $S_B$ or $S_W$. The first integral accounts for the potential disturbance due to blades and hub kinematics and shape whereas the second one describes the hydrodynamic effects associated to the vorticity layer (i.e. the potential wake) released behind the lifting blades.

In the framework of potential flows, the wake represents a zero-thickness layer departing from the trailing edge of lifting bodies where generated vorticity is shed downstream. Symbol $\Delta\varphi$ indicates the potential jump across $S_W$, whereas $G$ and $\partial G/\partial n$ are the unit source and dipole in the unbounded 3D space, respectively. Finally, $E(\mathbf{x})$ is a domain function defined as 1, 1/2 or 0 for $\mathbf{x}$ inside the flow-field, on the solid boundary surface or inside the solid body, respectively. Enforcement of Eq. 1 on the turbine surface yields a Boundary Integral Equation for the velocity potential where unknowns are distributed over the turbine surface ($\varphi$) and wake ($\Delta\varphi$). Impermeability condition on $S_B$ and the Kutta-Morino condition [25] on $S_W$ are introduced for the wellposedness of the problem. After discretization of $S_B$ and $S_W$ into surface panels and enforcement of Eq. 1 at the centroids of the body panels, the application of a zero-th order Boundary Element Method (BEM) yields a linear set of algebraic equations in terms of $\varphi$ on the body surface. The pressure field upon the blade(s) is then computed by the Bernoulli equation whereas rotor hydroloads (forces and moments) are carried out by integrating normal and tangential stresses

$$\mathbf{f} = \oint_{S_B}(p\mathbf{n}+\tau\mathbf{t})dS$$
$$\mathbf{m_o} = \oint_{S_B}[p(\mathbf{x}-\mathbf{x_0})\times\mathbf{n}+\tau(\mathbf{x}-\mathbf{x_0})\times\mathbf{t}]\,dS \quad (2)$$

where pressure $p$ and friction $\tau$ represent, respectively, normal and tangential stresses on $S_B$ whilst $\mathbf{n}$ and $\mathbf{t}$ are unit vectors normal and tangential to the blade(s) surface. Denoting by $\mathbf{e_x}$ the unit vector aligned to the turbine rotor axis, the delivered turbine thrust and torque are given by $T=\mathbf{f}\cdot\mathbf{e_x}$ and $Q=\mathbf{m_0}\cdot\mathbf{e_x}$ respectively. Note that the wake surface behind the rotor disk is unknown a priori and has to be computed as a part of the BEM computation to well predict the hydrodynamic loads on rotor blades. To this aim a wake-alignment procedure where wake points are moved with the local downstream velocity field is used, according to

the nonlinear (pseudo) lagrangian scheme described in [26] and successfully applied in the past for the aerodynamic analysis of a wind turbine in axial uniform inflow [22].

### B. *Numerical Results*

A three-bladed, 0.8 m diameter marine current turbine with NACA 66-8XX blade sections is investigated in the following. The turbine geometry is sketched in Fig. 1, where the definition of rotor radius $R$, blade chord $c$ and section twist $\theta$, are shown. Blade constructive twist angle and chord/radius ratio spanwise distributions are depicted in Figs. 2 and 3.

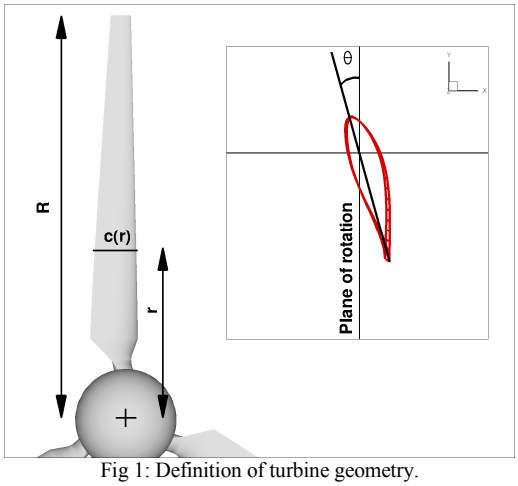

Fig 1: Definition of turbine geometry.

More details on MCT geometry are found in [18]. For an incoming water velocity $v_w = 1.73$ m/s and a tip speed ratio $TSR = \lambda = \omega_T R / v_w$ equal to 3 ($\omega_T$ denote the rotor angular velocity), Fig. 5 highlights the shape of the wake captured by the hydrodynamic computation performed through a blade spatial discretization of 40 chordwise panels, 60 spanwise panels and 540 wake panels. This type of mesh assures convergence results; hence, it is further used for the MCT hydrodynamic analysis at $\lambda$ values ranging from 3 to 12. Figs. 6a and 6b show the comparison, in terms of turbine power and torque coefficient, between performance predicted by the proposed hydrodynamic approach and those coming from available experiments and numerical data. Measurements, performed at the *QinetiQ* cavitation tunnel (*Haslar Marine Technology Park*), are obtained through a set-up in which the rotor is attached to a main shaft driving a DC generator. An in-line strain gauge dynamometer mounted next to the turbine is used to measure thrust and torque. The strain gauge bridge circuit is connected via a slip-ring assembly to conditioners, and output signals are acquired on a computer using a data acquisition system. The electrical power is absorbed with rheostats, which also allow regulation of the rotor speed (see [18] for details about the experimental set-up). Literature numerical results, herein provided as a reference, are obtained by applying a panel method-based formulation in which viscosity effects are modeled through section lift and drag forces derived from two-dimensional data (see [19]). In details, there is a good agreement in terms of thrust coefficient $C_T = 2T / \rho v_w^2 \pi R^2$ ($\rho$ is the water density) both with experiments and numerical data from [19]. Similar considerations hold for the power coefficient $C_P = 2Q\omega_T / \rho v_w^3 \pi R^2$ shown in Fig. 6 ; in this case, for $\lambda$ less than 8 the present approach yields a better agreement, whereas at higher values of the angular velocity literature results are closer to the experimental ones. Generally speaking, the trend of thrust and power coefficients carried out by the present approach are in satisfactory agreement with experiments; although the quality of the results is comparable with that associated to the numerical method proposed in [19], this comparison suggests that the different strategies used to model viscous effects may be more or less effective in relation to the $\lambda$ value.

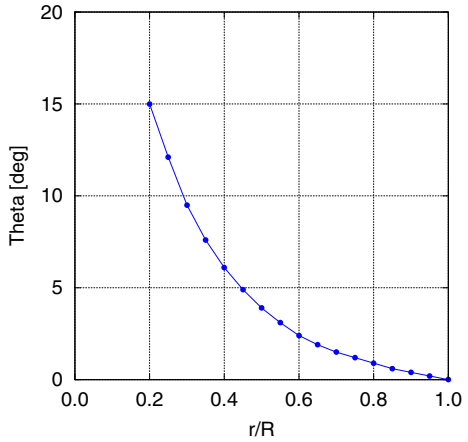

Fig 2: Spanwise distribution of blade constructive twist angle.

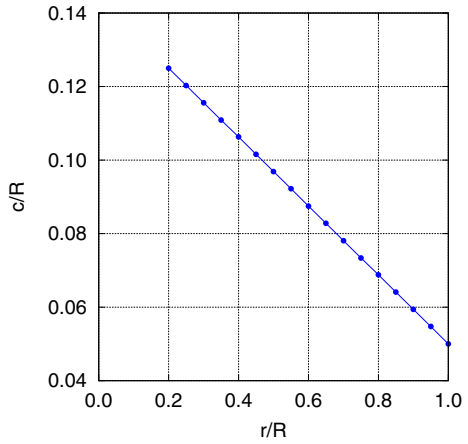

Fig 3: Spanwise distribution of nondimensional blade chord.

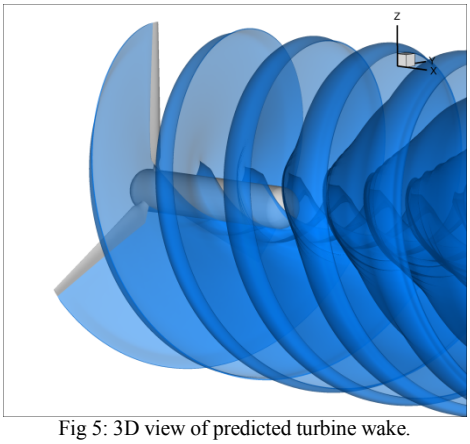


Fig 5: 3D view of predicted turbine wake.

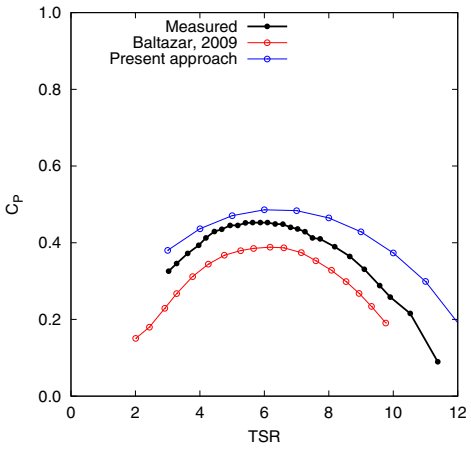


Fig. 6 Comparison between computed and experimental performance: power coefficient

The main parameters of the adopted turbine are summarized in Table I. The column "real turbine" contains the data of the turbine designed by BEM whereas the column "Turbine emulator" is referred to the emulator set-up of the laboratory used for testing the entire generation system. The mechanical values of the real turbine in Table I are those corresponding at the sea speed of 4 m/s which is supposed the maximum value of the sea speed. In particular, the rated power of 2 kW of the laboratory set-up corresponds to the power provided by the induction generator furnished at the rated torque of 12 Nm and rated speed of 150 rad/s. The resulting torque versus speed characteristics of the marine turbine, for several values of the sea speed, have been plotted in Fig. 7. It can be observed that at the maximum sea speed of 4 m/s, the turbine provides almost the rated torque of the induction machine but the corresponding maximum generable power is obtained at a turbine rated speed of about 90 rad/s which is much lower the maximum speed. Therefore the induction generator is fully exploited in terms of torque whereas it is underutilized in terms of speed. It can be noted that, to match the rated power of the experimental turbine to the corresponding turbine emulator, only the radius of the turbine has been modified. This does not affect anyhow the reliability of the obtained results.

TABLE I. MARINE TURBINE PARAMETERS

| | Real turbine | Turbine Emulator |
|---|---|---|
| R [m] | 0.8 | 0.15 |
| $\lambda_{opt}$ | 6 | 6 |
| $C_{pmax}$ | 0.46 | 0.46 |
| n | 0.5 | 0.5 |
| Generator rated power [kW] | 30 | 2 |
| Generator rated speed [rpm] | 1500 | 1500 |
| Blade pitch angle [deg] | 20 | 20 |
| Blades no. | 3 | 3 |

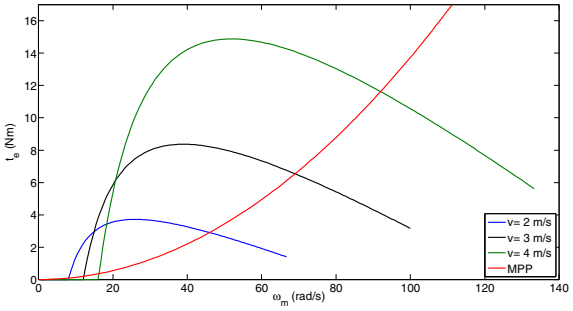


Fig. 7: Marine turbine torque vs speed characteristics

## C. *Marine turbine emulator*

In the proposed test setup, the marine turbine has been emulated experimentally by a torque controlled PMSM drive, whose speed-torque characteristics instantaneously reproduces those of a real marine turbine. The model adopted for emulating the turbine is described in the following.

The power generated by a marine turbine can be written as [18]:

$$P_m = 0.5 \cdot C_p(\lambda)\rho A \cdot v_w^{\ 3}$$

where $P_m$ is the mechanical power of the turbine in [W], $C_p$ is the power coefficient of the turbine, $\rho$ is the water density in [kg/m$^3$], $A$ is the turbine swept area in [m$^2$], $v_w$ is the sea speed in [m/s], $\lambda$ is the tip speed ratio defined as $\lambda = \omega_T R / v_w$, where $\omega_T$ is the turbine angular speed and $R$ is the turbine radius. In this case, the $C_p(\lambda)$ has been obtained by the above described BEM analysis of the marine turbine (Figs. 6a and 6b). The obtained BEM results have been interpolated by a 2$^{nd}$ order curve. This has been the function implemented in the DSP controlling the marine turbine emulator. Figure 7 shows the torque versus speed characteristics of the emulated marine turbine, obtained for different values of the sea speed, as well as the maximum power points at each machine rotating speed.

## III. Marine Generator Control Technique

### A. Machine side Converter with Field Oriented Control (FOC)

A high performance control technique of the induction machine has been chosen, in particular the Field Oriented Control (FOC) [27] so as to manage the turbine torque variations with the water speed. In the adopted FOC scheme (Figure 8) current control is performed in the rotor flux oriented reference frame. The DC link control is provided by the grid side inverter. On the direct axis, a flux control loop commands the current loop and a voltage control loop commands the flux loop to permit the drive to work automatically in the field weakening region by maintaining constant the product of the rotor flux amplitude and the absolute value of the rotor speed. On the quadrature axis, a speed loop controls the current loop. The reference speed of the machine corresponding to the maximum power generable from the system at a given marine speed is retrieved by the GNG based MPPT technique (described in section IV) which has as inputs the estimated torque and the measured speed of the machine and gives as output the machine reference speed.

All controllers used in the control loops are PI (Proportional Integral) type. An asynchronous space vectorial modulation (SVM) with $f_{PWM}$=5 kHz has been used to command the inverter.

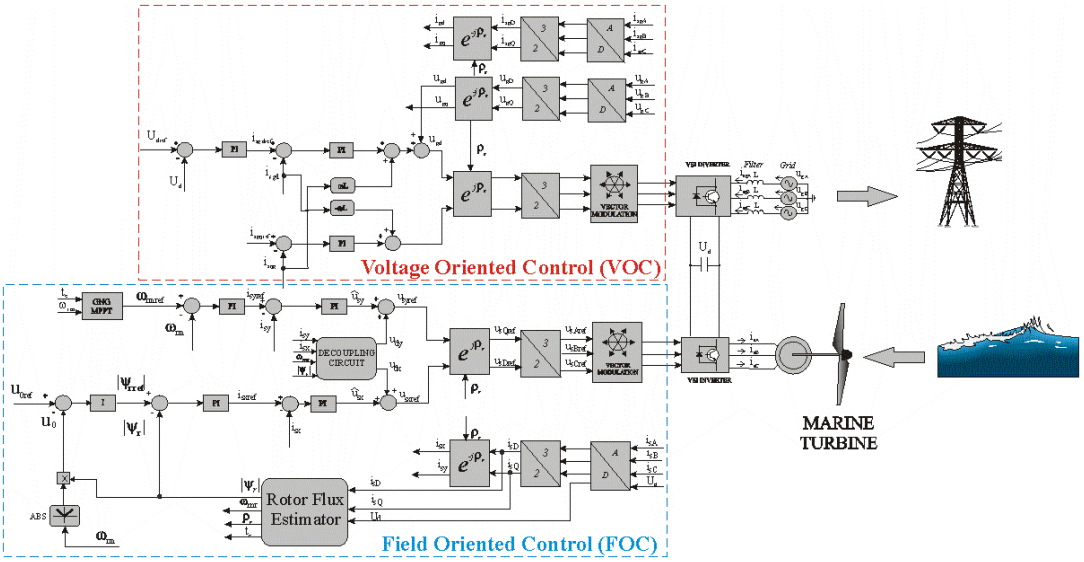


Fig. 8: Block diagram of the sea generator control scheme

### B. Grid side Converter with Voltage Oriented Control (VOC)

Grid side converter control has been performed on the basis of a high performance technique: Voltage Oriented Control (VOC) [28]. VOC is based on the idea of decoupling instantaneously the direct and quadrature components of the injected current, working in the grid voltage vector reference frame. Since the target here is to control directly the DC link voltage, the control scheme has been modified adding another control loop, the DC link voltage one whose output is the direct reference current. The quadrature reference current is always set to zero, so that the reactive power flow with the grid can be kept to zero. Also in this case, an asynchronous space vector modulation (SVM) technique with PWM frequency of 5 kHz has been adopted.

## IV. GNG Based MPPT

The basic idea of the proposed MPPT technique is to retrieve the optimal generator reference speed $\omega_{mrref}$ (meaning the speed corresponding to the maximum generable power) for any instantaneous value of the marine speed. This permits to have an MPPT technique based on speed control of the machine instead of its torque control, with all the consequent advantages in terms of safer and more stable operation of the entire system. To compute the optimal machine reference speed, it is necessary to estimate in advance the instantaneous values of the sea speed $v_w$. The knowledge of this variable is particularly important also for other features of the marine generator (it provides the information about the correct behaviour inside the minimum-maximum sea speed range and can thus command generator disconnections in case of need). Once the sea speed is estimated, the generator reference speed $\omega_{mrref}$ can be computed on the basis of the following expression:

$$\omega_{mrref} = n v_{stim} \lambda_{opt} / R ,$$

where $\lambda_{opt}$ is the optimal value of the tip speed ratio, which is a known quantity and dependent on the characteristics of the turbine, $v_{stim}$ is the estimated sea speed. For stability reasons, the optimal generator reference speed is not directly provided to the

machine control system, but a first order lag with time constant $\tau$ is introduced to avoid instability phenomena of the whole control system. The complete block diagram of the MPPT technique is shown in figure 9.

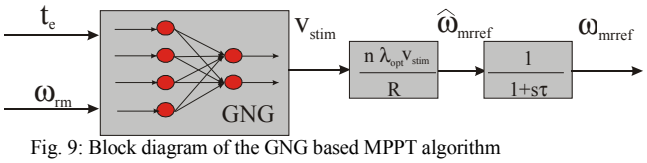


Fig. 9: Block diagram of the GNG based MPPT algorithm

To estimate the instantaneous sea speed $v_w$, the relationship between the generator torque $t_e$ and generator speed $\omega_{mr}$ is firstly computed on the basis of the model in section III, from which a complete training set of data has been created. This relationship has been then learnt off-line by a Growing Neural Gas (GNG) network [29] developed by the authors in Matlab®-Simulink® environment (full description of the GNG algorithm will be given in the final version of the work for lack of space here). A GNG with a maximum number of 1000 neurons has been used. After training, the GNG has been used on-line by exploiting the turbine characteristic function to be inverted. Figure 10 shows the turbine characteristic $t_e$ versus $v$ and $\omega_{mr}$ as well as the neurons created by the GNG (red) with the corresponding links (green). Furthermore, in magenta the points corresponding to the maximum generable power for each value of $v$ and $\omega_{mr}$ are also shown. It can be observed that the neurons cover entirely the turbine characteristic.

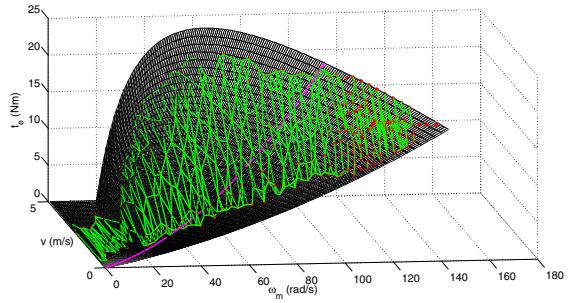


Fig. 10: Generator torque vs sea and machine speeds surface, GNG neurons (red) and links among neurons (green)

## V. Test Set-up

The employed test set up consists of two parts, respectively the grid side and machine side one. The grid side part is composed of the following items:

- A 8 kVA, three-phase VSI.
- A dSPACE card (DS1103) with a PowerPC 604e at 400 MHz and a floating-point DSP TMS320F240 for the control of the grid side inverter.
- An interconnection series inductance of 12 mH with a parasitic resistance of 0.9 Ω .

The machine side part is composed of the following items:

- A three-phase induction motor with parameters synthesized in Table II.
- A 8 kVA, three-phase VSI for the control of the machine side inverter.
- A brushless Interior Mounted Permament Magnets (IMPM) machine drive for emulating the wind turbine.
- A dSPACE card (DS1103) with a PowerPC 604e at 400 MHz and a floating-point DSP TMS320F240 for the control of the machine side inverter.

Fig.s 11 show two photographs of the test setup. As previously said, the marine turbine is suitably replaced by a wind turbine emulator whose operation can be summarized as follows. The marine turbine is substituted by a torque controlled PMSM drive.

TABLE II. Parameters of the Induction Motor

| | |
|---|---|
| Rated power $P_{rated}$ [kW] | 2.2 |
| Rated voltage $U_{rated}$ [V] | 220 |
| Rated frequency $f_{rated}$ [Hz] | 50 |
| Pole-pairs | 2 |
| Stator resistance $R_s$ [Ω] | 2.9 |
| Stator inductance $L_s$ [mH] | 223 |
| Rotor resistance $R_r$ [Ω] | 1.52 |
| Rotor inductance $L_r$ [mH] | 229 |
| 3-phase magnetizing inductance $L_m$ [mH] | 217 |
| Moment of inertia J [kg·m$^2$] | 0.0048 |

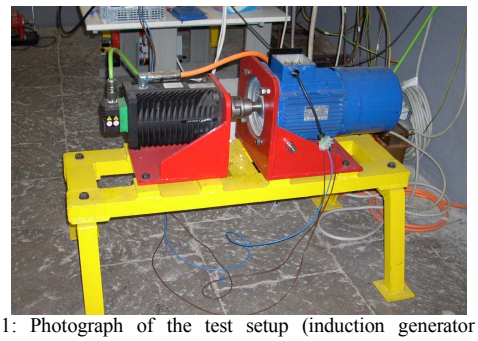

Fig. 11: Photograph of the test setup (induction generator + turbine emulator)

The PMSM drive receives in input the torque reference on the basis of the turbine model (see § II), which has as inputs the sea speed (given by the user) and the machine rotational speed (given by an encoder), In this way, the PMSM machine drive behaves exactly as the marine turbine for each value of the wind speed and the machine speed.

## VI. Experimental Results

The GNG based MPPT technique for marine generation system with induction machine has been experimentally implemented and verified on the test set-up described in section V. The marine generator is connected to the grid by a three-phase inductance of 12 mH. On the machine side DSP, the FOC scheme has been implemented as well as the MPPT algorithm with the marine turbine model described in section III. It should be minded that for the on-line implementation of the GNG only the recalling phase is to be considered, which is not particularly cumbersome. To show the goodness of the proposed MPPT technique, the following experimental test has been made. The marine generation system, initially working at steady-state at the sea speed of 4 m/s, has been given a set of sea speed variations (2→4 →2 →3 →4 m/s). Figure 12 shows the real sea speed and the corresponding one estimated by the GNG network.

It should be observed that the estimated speed properly tracks the real one and converges almost istantaneously to it. Correspondingly, figure 13 shows the reference and measured machine speed which are increased or decreased according to the increase or the decrease of the estimated sea speed to track the

MPP. Figures 14 and 15 show respectively the grid side $i_{sd}$, $i_{sq}$ reference and measured currents and the active ($P$) and reactive ($Q$) power flowing into the power grid. They show that both the $i_{sq}$ current and reactive power $Q$ are controlled to zero, highlighting that no reactive power exchange with the power grid exists. On the contrary, an increase of the $i_{sd}$ current component and the active power $P$ occurs at each increase of the sea speed as expected. Figure 16 shows the machine side $i_{sx}$, $i_{sy}$ reference and measured currents. As expected, the $i_{sx}$ remains constant showing a constant magnetization of the machine, while $i_{sy}$ exhibits a negative step variation at each increase of the sea speed (motoring convention sign has been adopted here). Finally, Figure 17 shows the torque versus speed characteristic of the turbine at the initial and final sea speed values as well as the steady-state maximum power curve (red) and the transient locus described by the machine torque versus speed. It should be noted that the starting and ending points of this locus lie on the corresponding turbine characteristics as well as on the maximum power trajectory, showing the effectiveness of the proposed approach. This is confirmed by the power versus speed curve shown in figure 18, which assesses that the proposed MPPT permits the generator to track the maximum power points of each characteristic.

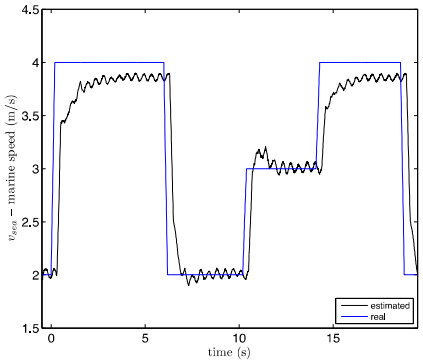


Fig. 12: real and estimated marine speed

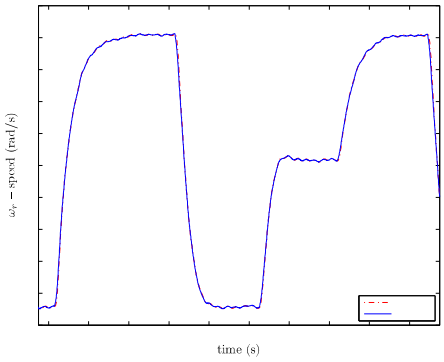


Fig. 13: reference and measured machine speed

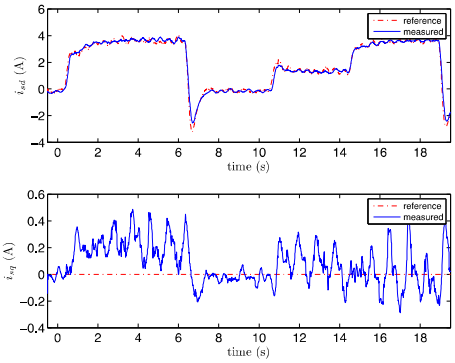


Fig. 14: grid side $i_{sd}$, $i_{sq}$ reference and measured currents

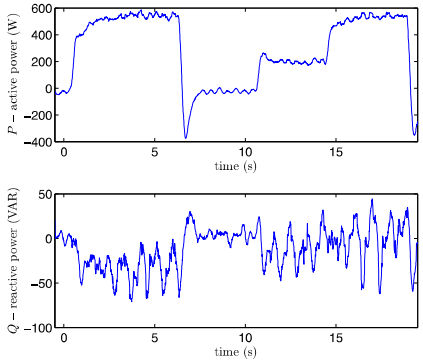


Fig. 15: Active ($P$) and reactive ($Q$) power exchanged with the power grid

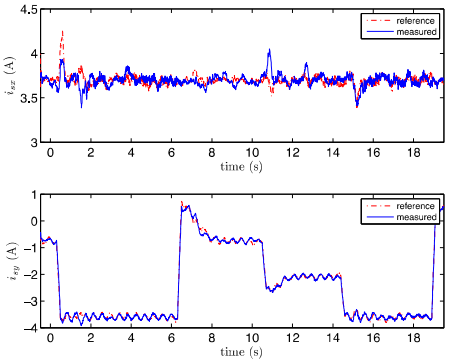


Fig. 16: Machine side $i_{sx}$, $i_{sy}$ reference and measured currents

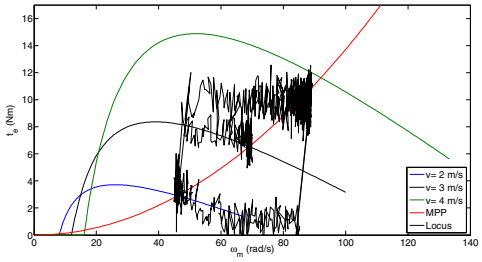


Fig. 17: torque vs speed locus

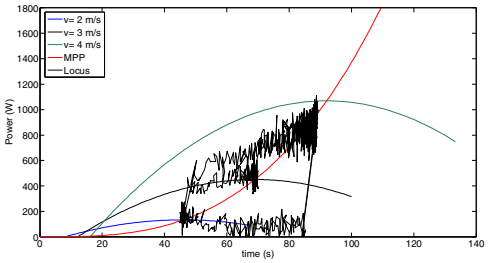


Fig. 18: Power vs speed locus

## VII. CONCLUSIONS

This paper presents a MPPT technique for high performance marine current generator with induction machine based on the Growing Neural Gas (GNG) network. The marine turbine characteristic curve has been firstly predicted by a BEM hydrodynamic formulation. On the basis of the results, the turbine mathematical model has been deduced permitting the turbine emulator to be tuned and the GNG network to be trained. Then a GNG network has been trained off-line to learn the turbine characteristic surface torque versus sea speed and machine speed, and implemented on-line to obtain the sea speed on the basis of the estimated torque and measured machine speed (surface function inversion). The machine reference speed is finally computed on the basis of the optimal tip speed ratio. For the experimental application, a back-to-back power converter configuration with two voltage source converters has been considered. Each converter has been controlled with a high performance vector control technique, respectively Field Oriented Control (FOC) and Voltage Oriented Control (VOC). A test setup has been built for the experimental assessment of the methodology. The marine turbine has been experimentally emulated with a PMSM drive, controlled in torque,. Experimental results show the correct behaviour of the proposed MPPT technique which permits to instantaneously estimate the sea speed and correspondingly to compute the optimal machine reference speed for tracking the maximum available power.

## REFERENCES


[1] G. A.S. Bahaj, L.E. Myers, “Fundamentals applicable to the utilisation of marine current turbines for energy production”, Ren. En. 28 (2003) 2205–2211

[2] A.S. Bahaj, W.M.J. Batten, G. McCann , “Experimental verifications of numerical predictions for the hydrodynamic performance of horizontal axis marine current turbines”, Renewable Energy, Volume 32, Issue 15, December 2007, Pages 2479–2490.

[3] L. Myers, A.S. Bahaj, “Power output performance characteristics of a horizontal axis marine current turbine”, Ren. En. 31 (2006) 197–208.

[4] W.M.J. Batten , A.S. Bahaj , A.F. Molland , J.R. Chaplin, “Hydrodynamics of marine current turbines”, Renewable Energy 31 (2006) 249–256.

[5] Ye Li, Barbara,J. Lence, , Sander,M.Calisal, “Modeling tidal turbine farm with vertical axis tidal current turbines”, IEEE International Conference on Systems, Man and Cybernetics, 2007. ISIC. Montreal, Que. 7-10 Oct. 2007.

[6] Jai N. Goundar, M. Rafiuddin Ahmed, “Design of a horizontal axis tidal current turbine”, Applied Energy 111 (2013) 161–174.

[7] R. Vennell, “Exceeding the Betz limit with tidal turbines”, Renewable Energy 55 (2013) 277-285

[8] W.M.J. Batten, A.S. Bahaj, A.F. Molland, J.R. Chaplin, “The prediction of the hydrodynamic performance of marine current turbines”, Renewable Energy 33 (2008) 1085–1096

[9] M.J. Khan, G. Bhuyan, M.T. Iqbal, J.E. Quaicoe, “Hydrokinetic energy conversion systems and assessment of horizontal and vertical axis turbines for river and tidal applications: A technology status review”, Applied Energy 86 (2009) 1823–1835

[10] S.E. Ben Elghali, M.E.H. Benbouzid, J.-F. Charpentier, “Modelling and control of a marine current turbine-driven doubly fed induction generator”, IET Renew. Power Gener., 2010, Vol. 4, Iss. 1, pp. 1–11.

[11] R. Datta and V. T. Ranganathan, “Variable-speed wind power generation using doubly fed wound rotor induction machine—A comparison with alternative schemes,” IEEE Trans. Energy Convers., vol. 17, no. 3, pp. 414– 421, Sep. 2002.

[12] S. Benelghali, M. El Hachemi Benbouzid, J. Charpentier,” Generator Systems for Marine Current Turbine Applications: A Comparative Study, , IEEE Journal of Oceanic Engineering, vol 37, no 3,July 2012.

[13] S.M. Mousavi G., “An autonomous hybrid energy system of wind/tidal/microturbine/battery storage”, Electrical Power and Energy Systems 43 (2012) 1144–1154,

[14] N. Khan, S.F. Rabbi, M. J. Hinchey, M.A. Rahman, “An adaptive nonlinear MPPT controller for stand alone marine current energy conversion systems”, IECON 2013 - 39th Annual Conf. of the IEEE Industrial Electronics Society, 2013, Vienna, Austria, November 10-13, 2013

[15] M. Cirrincione, M. Pucci, G. Vitale, “Growing Neural Gas (GNG)-Based Maximum Power Point Tracking for High-Performance Wind Generator With an Induction Machine”, IEEE Trans. On Ind. Appl. , vol. 47, no. 2, March/April 2011

[16] M. Cirrincione, M. Pucci, G. Vitale, "Neural MPPT of Variable Pitch Wind Generators with Induction Machines in a Wide Wind Speed Range", IEEE Trans. on Ind. Appl. , VOL. 49, NO 2, March/April 2013.

[17] M. Cirrincione, M. Pucci, G. Vitale, "Growing Neural Gas based MPPT of Variable Pitch Wind Generators with Induction Machines", IEEE Trans. on Ind. Appl., vol. 48, n. 3, May/June 2012.

[18] A.S. Bahaj, A.F. Molland, J.R. Chaplin, W.M.J. Batten, “Power and thrust measurements of marine current turbines under various hydrodynamic flow conditions in a cavitation tunnel and a towing tank,” *Renewable Energy*, (2007), Vol. 32, Issue 3, 407-426.

[19] J. Baltazar, J.A.C. Falcão de Campos, “Unsteady Analysis of a Horizontal Axis Marine Current Turbine in Yawed Inflow Conditions With a Panel Method,” Proceedings of the *First International Symposium on Marine Propulsors (SMP’09)*, (2009), Trondheim, Norway.

[20] A. Calabretta, M. Molica Colella, L. Greco, G. Dubbioso, C. Testa, and M. Gennaretti, “A comprehensive numerical model for horizontal axis wind turbines Aeroelasticity”, Proceedings of the *Conference on Wind Energy Science and Technology*, (2013), Ankara (Turkey).

[21] A. Calabretta, M. Molica Colella, L. Greco, M. Gennaretti, “Assessment of aerodynamics models for wind turbines aeroelasticity,” Proceedings of the *2014 World Congress on Advances in Civil, Environmental, and Materials Research (ACEM14)*, (2014), Busan (Korea).

[22] L. Greco, C. Testa, and F. Salvatore, “Design Oriented Aerodynamic Modelling of Wind Turbine Performances”, *Journal of Physics*, Conference Series, (2007), Vol. 75(1).

[23] J.S. Carlton, “Marine Propellers and Propulsion,” Butterworth-Heinemann Ltd., (2012) (Third Ed.).

[24] C.W.B. Grigson, “A Planar Friction Algorithm and its Use in Analysing Hull Resistance,” *Trans. of the Royal Inst. of Nav. Arch. (RINA)*, (2000), Vol. 142, 76-115.

[25] L. Morino, “Boundary Integral Equations in Aerodynamics,” *Appl. Mechanics Reviews*, (1993), Vol. 46(8), 445-466.

[26] L. Greco, R. Muscari, C. Testa, and A. Di Mascio, “Marine Propellers Performance and Flow-Field Features Prediction by a Free-Wake Panel Method”, Journal of Hydrodynamics, Ser. B , (2014), (in press).

[27] P. Vas, Sensorless Vector and Direct Torque Control, Oxford Science Publication, 1998.

[28] M.P. Kazmierkowski, R. Krishnan and F. Blaabjerg, Control in Power Electronics, London, UK, 2002.

[29] B. Fritzke, “Growing Cell Structures – a self-organizing network for unsupervised and supervised learning”, Neural Networks, 7(9), 1994, pp. 1441-1460.